Interaction between an atom and a mesoscopic helicoidal system. Fourier-transform analysis

E. Alvira, J. Breton, and V. Delgado
Departamento de Fisica Fundamental y Experimental, Universidad de La Laguna, 38203 La Laguna, Tenerife, Spain

C. Girardet
Laboratoire de Physique Molèculaire, Unité No. 772 associée au Centre National de la Recherche Scientifique Université de Franche-Comté, La Bouloie, 25030 Besançon Cedex, France

(Received 5 June 1992; accepted 20 July 1992)

A Fourier-transform analysis (FTA) of the interaction potential between an atom and a helicoidal periodic distribution of atoms is presented. The accuracy of this procedure is tested with respect to the standard pairwise potential sum techniques. It is shown that the convergence of FTA is quite good, mainly when the probe atom lies inside the helicoidal cavity and when the matter density on the helix remains reasonably large. Criteria are given for the applicability of the FTA to a helicoidal atomic distribution.

I. INTRODUCTION

The interaction between an atom or a molecule and a mesoscopic system has been widely studied for particularly simple geometries of the system. As an example, the interaction potential between an adatom and a substrate is generally written[1] as an extended sum of pairwise atom–atom contributions. The need for accurate calculations of the energy on the one hand and for fast sum procedures on the other hand requires the use of computational techniques based on approximate schemes. Beyond the most commonly used continuum approximation, the two-dimensional (2D) Fourier analysis of the interaction potential has been developed by Steele[2] for infinite periodic planar structures. The accuracy of this analysis depends on the truncation of the sum over the reciprocal translation vectors **g** which itself strongly depends on the matter density in the planes.

However, there is now a reverse tendency which consists in assessing the role of the reduced dimensionality on the bonding properties of matter, particularly in confinement effects on physisorption. In that case, the surface geometry can be spherical, cylindrical, or even helicoïdal, and the previously mentioned 2D Fourier analysis appears more complicated. Zeolite and related compound micropores are illustrative examples of particular surface geometries. Atom or molecule transport and adsorption on these confined surfaces have been shown[3] to depend significantly on these geometries and also on the framework structure and on long-range electrostatic fields found in many zeolites. Accurate calculations of the interaction energy between the adsorbate and the sorbent thus accumulate two species of difficulties tied to the extended potential sum procedure and to the particular surface geometry. Another example for which extended interaction calculations are required concerns the ion and atom diffusion in solids with low-order symmetry. The crystals pertaining to quartz family are formed by atomic helicoïdal distribution forming channels which allow the particles to migrate, as observed in sweeping experiments.[4] The atomic probe of polymers or of biological molecules (DNA, RNA, proteins, etc.) as in atomic force microscopy, is a third example for which it is necessary to get accurate information on the interaction potential between an atom and a helicoidal extended system. The extension to a chiral molecule interacting with a biological molecule can also provide an interpretation of the chiral discrimination observed in chromatography experiments[5] or of the structures of biological systems.[6]

In this paper, we develop a Fourier-transform analysis procedure (FTA) of the interaction energy between an atom and an helicoidal atomic structure. In contrast with planar geometries for which the periodicity is described by a 2D cell, the periodicity of the helicoidal system is determined by the 1D cell characterizing the length of the helix segment, i.e., the distance between equivalent atoms along the helix. The helix geometry and the probe atom position are defined in Sec. II. The general expression of the interaction potential is then given in Sec. III with particular attention to the case of a Lennard-Jones pairwise interaction. In Sec. IV, we consider first the analytical case where the probe atom remains on the helix axis and then compute the Fourier coefficients for a probe atom lying in a plane perpendicular to the helix axis. In both cases, the results on the Fourier analysis of the interaction energy are compared with those obtained in the standard sum procedure. A detailed discussion of the FTA method convergence, mainly on the g truncation, is done and the potential-energy surfaces are drawn for several helix characteristics.

II. GEOMETRY OF THE HELICOIDAL STRUCTURE

Let us consider identical atoms regularly distributed on a helix with pitch B and radius ρ and define the atom number N per helix pitch. The distance on the helix between two consecutive atoms on the helix is S_h and its projections on the helix axis and in a plane perpendicular to the helix axis are defined as b and a, respectively. b and a are respectively equal to $(B/2\pi)\ \theta_h$ and $\rho\theta_h$, where θ_h is the angle defining the small element a (see Fig. 1). The

 0021-9606/92/216821-08$006.00

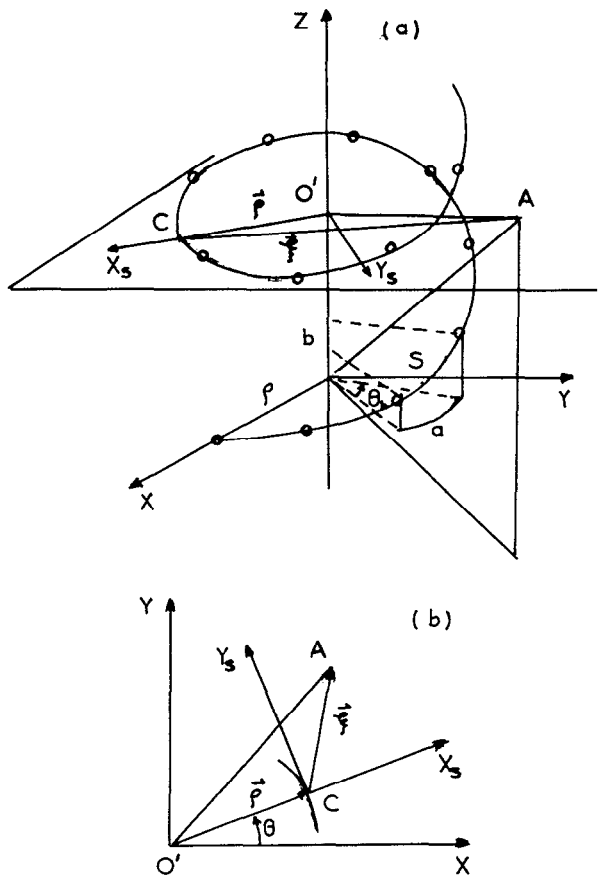

FIG. 1. Helix geometry in (a) the absolute frame (X,Y,Z) and (b) position of the probe atom in a plane perpendicular to the helix axis.

absolute frame (**X**,**Y**,**Z**) is such that the **Z** axis corresponds to the helix axis and the **X** axis lies in a plane perpendicular to the helix axis. The **X** axis is chosen along the vector joining the helix axis to the intersect point of the helix framework with this plane. We assume that there is an atom at the intersection of the helix and of the plane defined by the coordinates $(\rho,0,0)$. The helix structure is defined as

$$x=\rho\cos\theta,$$
$$y=\rho\sin\theta, \tag{1}$$
$$z=\frac{B}{2\pi}\theta.$$

The atom number N per pitch and the distance S_h between consecutive atoms are written as

$$N=B/b=2\pi\rho/a, \tag{2}$$
$$S_h=[(2\pi\rho)^2+B^2]^{1/2}/N=1/N\eta,$$

where η^{-1} characterizes the inverse of the length of an helix pitch. Note that N is not necessarily integral. The position of the nth atom on the helix can be written in terms of the curvilinear coordinate S_n,

$$S_n=nS_h \quad (n \text{ integer}). \tag{3}$$

S_h thus appears as the modulus of the primitive vector in the curved direct space, and the reciprocal primitive vector is defined as

$$G_g=2\pi g/S_h \quad (g \text{ integer}). \tag{4}$$

S_h, S_n and S represent distances measured along the helix. Let us then define the position $\mathbf{R}(X,Y,Z)$ of the probe atom A. The plane $Z=$const containing this atom intersects the helix at a point C which is at a distance S from the helix origin $(\rho,0,0)$, and the helix axis at a point O'. Inside this plane, the position of atom A is [Fig. 1(b)]

$$\mathbf{O'A}=\boldsymbol{\rho}(S)+\boldsymbol{\xi}(S), \tag{5}$$

where $\boldsymbol{\rho}(S)$ defines the helix vector $\mathbf{O'C}$ in the absolute frame,

$$\boldsymbol{\rho}(S)=\rho\cos\theta(S)\mathbf{X}+\rho\sin\theta(S)\mathbf{Y}$$

and $\boldsymbol{\xi}(S)$ characterizes the vector $\mathbf{CA}$ whose components ξ_X and ξ_Y in the moving frame $(\mathbf{X}_S,\mathbf{Y}_S)$ are S independent, while their components in the absolute frame are written,

$$\hat{\xi}_X=\cos\theta(S)\xi_X-\sin\theta(S)\xi_Y, \tag{6}$$
$$\hat{\xi}_Y=\sin\theta(S)\xi_X+\cos\theta(S)\xi_Y.$$

The angle $\theta(S)$ which defines the orientation of the vector $\mathbf{O'C}$ is given by

$$\theta(S)=\frac{2\pi}{B}Z=2\pi\eta S. \tag{7}$$

The position of the probe atom is finally determined by its components in the absolute frame as

$$X=(\rho+\xi_X)\cos 2\pi\eta S-\xi_Y\sin 2\pi\eta S,$$
$$Y=(\rho+\xi_X)\sin 2\pi\eta S+\xi_Y\cos 2\pi\eta S, \tag{8}$$
$$Z=B\eta S.$$

Note also the following relation, which will be useful later:

$$(\xi)^2=(X-\rho\cos 2\pi\eta S)^2+(Y-\rho\sin 2\pi\eta S)^2. \tag{9}$$

III. EXPRESSION OF THE INTERACTION POTENTIAL

A. General expression

The interaction energy between the probe atom A and the helix assumed to be infinite is a periodic function of the S variable. By means of Eq. (8), we have defined a set of curvilinear coordinates such that this potential energy verifies

$$V(S+S_n,\xi)\equiv V(S,\xi) \tag{10}$$

at fixed ξ_X and ξ_Y. Let us recall that S_n defines the position of the nth atom along the helix [Eq. (3)]; therefore, the periodicity is over the S variable, not necessarily in Z and θ, leading to arbitrary N values [Eq. (2)]. V can therefore be expanded in a Fourier series as

$$V(S,\xi)=\sum_g W_g(\xi)e^{iG_gS}. \tag{11}$$

The Fourier expansion is performed in the curvilinear reciprocal space as discussed before, and the Fourier coefficients are given by

$$W_g(\xi)=\frac{1}{S_h}\int_S dS\exp\left(-i2\pi g\frac{S}{S_h}\right)V(S,\xi), \tag{12}$$

where the integration is done over a period of the variable S.

The interaction between the A atom and the helicoidal system can be written as a sum of pairwise potentials $v_n(R_n)$ where R_n characterizes the distance between A and the nth helix atom, as

$$V(s,\xi)=\sum_n v_n(S-S_n,\xi). \tag{13}$$

Equation (13) can be replaced into the Fourier coefficient $W_g(\xi)$ [Eq. (12)], which becomes

$$W_g(\xi)=\frac{1}{S_h}\sum_n\int_S e^{-i2\pi g(S-S_n)/S_h}v_n(S-S_n,\xi). \tag{14}$$

In Eq. (14), we have artificially introduced the unit factor $\exp(i2\pi gS_n/S_h)$ in order to define the new variable $t=S-S_n$. Moreover, it is straightforward to show that the integration over S for fixed n is equivalent to the integration over S_n for fixed S. Equation (14) thus becomes

$$W_g(\xi)=\frac{1}{S_h}\int_{\text{helix}} dS_n e^{-i2\pi gt/S_h}v(t,\xi), \tag{15}$$

where we have used the identity $\Sigma_n\int_{S_n}=\int_{\text{helix}}$. From Eq. (2), the Fourier coefficient is finally written as

$$W_g(\xi)=N\eta\int_{\text{helix}} dt e^{-i2\pi gN\eta t}v(t,\xi), \tag{16}$$

and, v being real, separated into real and imaginary parts $W_g^R(\xi)$ and $W_g^I(\xi)$ obeying the relations

$$W_{-g}^R\equiv W_g^R,\quad W_{-g}^I\equiv -W_g^I. \tag{17}$$

The zero-order Fourier coefficient valid for the continuum approximation is given by

$$W_0(\xi)=N\eta\int_{\text{helix}} dt\, v(t,\xi). \tag{18}$$

From Eqs. (11), (16), (17), and (18), the interaction energy between the A atom and the helix is

$$V(s,\xi)=W_0(\xi)+2\sum_{g>0}(W_g^R\cos 2\pi g\eta S+W_g^I\sin 2\pi g\eta S). \tag{19}$$

V depends on the interaction parameters [through $v_n(R_n)$] between the A atom and a helix atom, on the helix parameters (ρ,B), and on the atom number density along the helix.

Note that this expression V has been determined by assuming that all the atoms are identical. The model could, however, be generalized to an helix with several atom species by considering a larger primitive vector containing the different atoms.

B. Application to a Lennard-Jones pairwise potential

Equation (19) is quite general and independent of the form of the interaction potentials between the A atom and a helix atom. In this section, we assume a Lennard-Jones form for the pairwise interaction,

$$v(S-t,\xi)=\sum_{k=6,12}(-)^{k/2}\frac{C_k}{d^k(S-t,\xi)}, \tag{20}$$

where the C_k's are the usual Lennard-Jones coefficients and d characterizes the distance between the A atom and a helix atom defined by its position $(\rho\cos 2\pi\eta t,\ \rho\sin 2\pi\eta t,\ B\eta t)$,

$$d^2(S-t,\xi)=(X-\rho\cos 2\pi\eta t)^2+(Y-\rho\sin 2\pi\eta t)^2+[B\eta(S-t)]^2. \tag{21}$$

It is straightforward to show that Eq. (21) can also by written as [cf. Eqs. (8) and (9)]

$$d^2(S-t,\xi)=[\xi_x^S+\rho(1-\cos 2\pi\eta(S-t))]^2+[\xi_y^S+\rho\sin 2\pi\eta(S-t)]^2+[B\eta(S-t)]^2. \tag{22}$$

The Fourier coefficients are thus given, in that case, by

$$W_g^R(\xi)=\sum_{k=6,12}N\eta\int_{-\infty}^{+\infty}dt\cos 2\pi gN\eta(S-t)\times\frac{(-)^{k/2}C_k}{d^k(S-t,\xi)},\quad g\geqslant 0, \tag{23}$$

$$W_g^I(\xi)=\sum_{k=6,12}N\eta\int_{-\infty}^{+\infty}dt\sin 2\pi gN\eta(S-t)\times\frac{(-)^{k/2}C_k}{d^k(S-t,\xi)},\quad g>0.$$

An analytic calculation of these coefficients is tractable only for special positions of the A atom, for instance, along the helix axis. Otherwise, the expression of the distance d [Eq. (22)] is too complicated to allow us a complete analytical treatment and a numerical computation of the integrals in Eq. (23) is required.

IV. RESULTS AND DISCUSSION

A. The *A* atom located on the helix axis

When the probe atom lies in a confined geometry, inside the helix and along the helix axis, one has $\xi=-\rho$ or $X=Y=0$. The distance d [Eq. (21)] is simply written as

$$d(t)=[\rho^2+(B\eta t)^2]^{1/2}, \tag{24}$$

and the nonvanishing Fourier coefficients become

$$W_0=\sum_{k=6,12}\frac{2N}{B}\int_0^\infty du(-)^{k/2}\frac{C_k}{(\rho^2+u^2)^{k/2}}, \tag{25}$$

$$W_g^R=\sum_{k=6,12}\frac{2N}{B}\int_0^\infty du\cos 2\pi g\frac{N}{B}u\times\frac{(-)^{k/2}C_k}{(\rho^2+u^2)^{k/2}}.$$

The odd Fourier coefficients W_g^I are zero because of the parity of the potential with respect to the new variable $u=\beta\eta t$. The analytical integration is performed,[7] leading to

$$W_0=\frac{3\pi}{8}\frac{N}{B}\left(-\frac{C_6}{\rho^5}+\frac{21}{32}\frac{C_{12}}{\rho^{11}}\right), \tag{26}$$

$$W_g^R=\frac{\pi}{8}\frac{N}{B}e^{-2\pi N\rho/B}\left[-\frac{C_6}{\rho^5}S_6(4\pi gN\rho/B)\right.$$

$$\left.+\frac{1}{64}\frac{C_{12}}{\rho^{11}}S_{12}(4\pi GN\rho/B)\right], \quad g>0,$$

where the function $S_i(x)$ is defined as

$$S_i(x)=\frac{1}{(i/2-1)!}\sum_{j=0}^{i/2-1}\frac{(i-j-2)!}{j!(i/2-j-1)!}x^j, \quad i=6,12. \tag{27}$$

Equations (26) exhibit a linear dependence in the ratio $N/B=b^{-1}$. Since b defines the distance between consecutive atoms projected on the helix axis, small values of b, i.e., large atomic number density, lead to large values of the Fourier coefficients whereas large values of b tend to decrease the magnitude of these coefficients. Moreover, the W_g coefficients depend strongly on the helix radius, the attractive contribution being trivially dominant for large values of ρ and the repulsive one for small values of ρ. Note also the exponential behavior of the coefficients $W_{g\neq 0}$ which significantly decrease for large values of g, N/B, and ρ. The dependence of the exponential factor in terms of the product $g(N/B)$ illustrates the fact that the convergence is better when N/B is large since the coefficients with increasing values of g vanish rapidly. On the contrary, it is necessary to take in account larger values of g when the atomic number density decreases.

The interaction energy between the probe atom and the helix can be written in terms of star quantities as

$$V^*(Z^*)=\frac{3\pi}{8b^*}(-\rho^{*-5}+21\rho^{*-11}/32)$$

$$+\frac{\pi}{8b^*}\sum_{g>0}e^{-2\pi g\rho^*/b^*}\cos 2\pi gZ^*/b^*$$

$$\times[\rho^{*-5}S_6(4\pi g\rho^*/b^*)$$

$$+\tfrac{1}{64}\rho^{*-11}S_{12}(4\pi g\rho^*/b^*)], \tag{28}$$

where $V^*=V/\epsilon$, $Z^*=Z/\sigma$, $\rho^*=\rho/\sigma$, $B^*=B/\sigma$, and $b^*=B/N\sigma$ are reduced quantities with respect to the standard Lennard-Jones parameters ϵ and σ.

We give in Table I the maximum values g_m of g, which are required to fit the absolute minima of the interaction energy V^* [Eq. (28)] to those determined by the standard sum procedure; the interaction energy obtained in this latter case is labeled V_{AA}^*. The fit is such that $\delta = V_{AA}^* - V^*$ remains smaller than 10^{-3}, for various values of ρ^* and b^{*-1}. For small b^* and/or large ρ^* values, the atomic helix distribution appears nearly as a continuum and the accuracy is very good for $g_m\leqslant 1$. For the reverse conditions (large b^* and small ρ^*), the convergence can be very bad and it is necessary to sum over g up to 60 since the matter looks quite discrete. Note also that for very small values of ρ^* ($\rho\simeq 0.5\sigma$), the potential V_{AA}^* becomes repulsive and the Fourier coefficients rapidly decrease down to zero, leading to inaccuracies.

TABLE I. Test of convergence of the Fourier analysis: maximum values g_m of g.

	b^*				
ρ^*	0.5	1	2	5	10
0.5	3[a]	8	16	41	60
1	1	2	4	11	21
2	1	1	1	2	5
5	1	1	1	1	1
10	1	1	1	1	1

[a]For these values of b^* and ρ^*, the interaction energy is repulsive when the probe atom lies on the helix axis. The value g_m corresponds to $\delta=10^{-2}$ instead of 10^{-3}.

Figures 2(a) and 2(b) exhibit the behavior of V^* for $b^*=2$ and two values of $\rho^*=1$ and 2, respectively, when

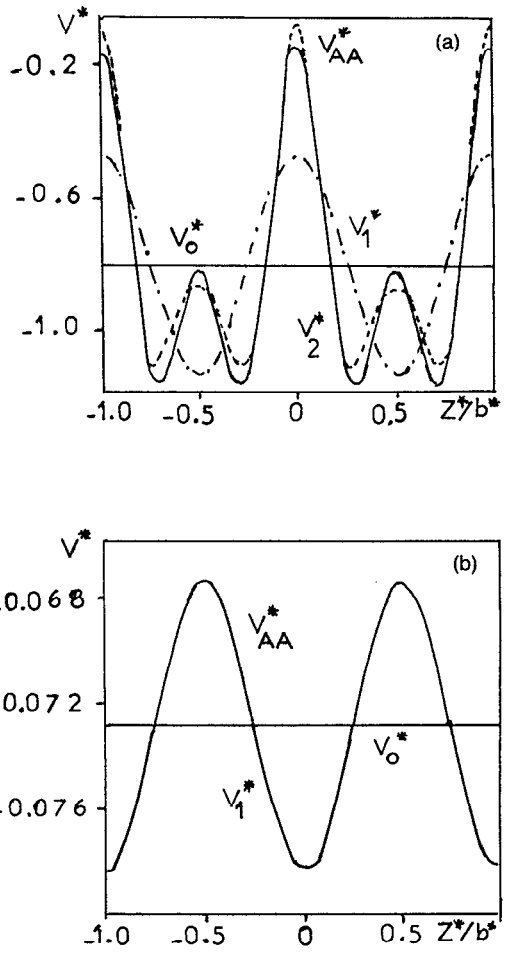

FIG. 2. Potential energy V^* experienced by the probe atom moving along the helix axis Z. Comparison between the standard sum procedure V_{AA}^* and the FTA $V_{g_m}^*$ with various truncations $g_m=0$, 1, 2; (a) $b^*=2$, $\rho^*=1$; (b) $b^*=2$, $\rho^*=2$. See the text for the definition of the reduced quantities.

the probe atom moves along the helix axis from $-b^*$ to $+b^*$. The helix atoms are located at $-b^*$, $-b^*/2$, 0, $b^*/2$, and b^*. The solid curves are drawn by taking into account the zero Fourier coefficient (V_0^*), the first two (V_1^*) and the first three (V_2^*) coefficients. They are compared to the interaction energy V_{AA}^* determined from the standard sum procedure. It is obvious from Fig. 2(a) that, when $\rho^*=1$, the g truncation at $g_m=2$ is required to reproduce a correct behavior of the minima and maxima of the potential-energy surface. Note that there are two maxima at $Z^*=Z/\sigma=0$ and $Z^*=b^*$ with a relative maximum at $b^*/2$, whereas two minima occur at $Z^*=b^*/4$ and $3b^*/4$. As mentioned before, the Fourier analysis is quite good for $g_m=4$ (Table I). When $\rho^*=2$ [Fig. 2(b)], the total interaction potential experienced by the probe atom is smaller than for $\rho^*=1$, because of the increase of the helix radius. In this case, the g truncation at $g_m=1$ is sufficient to reproduce in a quite good way the interaction potential surface V_{AA}^*. Note also that a single maximum occurs at $Z^*=b^*/2$, whereas the minima lie at $Z^*=0$ and $Z^*=b^*$.

B. The *A* atom located in a plane normal to the helix axis

1. General expression and symmetry properties

Let us consider a plane perpendicular to the helix axis located at the height Z_0, or equivalently at a distance S_0 from the helix origin. Equations (22) and (23) are then valid after replacing S by S_0. The change of variable $u=\beta N(S_0-t)$ leads to the Fourier coefficients expressed as

$$W_0=\frac{N}{B}\int_{-\infty}^{+\infty} du \sum_{k=6,12}(-)^{k/2}\frac{C_k}{d^k(u,\xi)}, \tag{29}$$

$$W_g^{R,I}=\frac{N}{B}\int_{-\infty}^{+\infty} du \begin{matrix}\cos\\ \sin\end{matrix}\left(2\pi\frac{N}{B}u\right)\sum_{k=6,12}(-)^{k/2}\frac{C_k}{d^k(u,\xi)}$$

with

$$d^2(u,\xi)=\left[X-\rho\cos\frac{2\pi}{B}(Z_0-u)\right]^2+\left[Y-\rho\sin\frac{2\pi}{B}(Z_0-u)\right]^2+u^2. \tag{30}$$

A tractable analytical procedure of integration for the Fourier coefficients is not possible and we must use numerical computations. However, the potential-energy surface exhibits symmetry properties which lead to simplifications. The change of variables:

$$\begin{aligned} X&=X'\cos 2\pi h/B-Y'\sin 2\pi h/B,\\ X&=X'\sin 2\pi h/B+Y'\cos 2\pi h/B,\\ Z_0&=Z'+h, \end{aligned} \tag{31}$$

where h is a real number, does not modify the distance d [Eq. (30)]. The identities then hold for the real and imaginary parts of the Fourier coefficients:

$$W_g^{R,I}(X,Y,Z_0)=W_g^{R,I}(X',Y',Z'), \tag{32}$$

TABLE II. Helix characteristics and Lennard-Jones coefficients.[a]

	ρ^*	B^*	N	C_6 (eV·Å^6)	C_{12} (eV Å^{12})
a	1.31	2	6	20	1.6×10^4
b	1.31	1.31	6	20	1.6×10^4
c	1.31	2	12	20	1.6×10^4
d	1	1.5	6	30	1.22×10^5

[a]The Lennard-Jones parameters σ and ϵ are 3 Å and 6.25 meV for cases *a*, *b*, and *c* and 4 Å and 1.84 meV for case *d*, respectively.

and the interaction potential between the probe atom and the helix is written as [cf. Eq. (19)]

$$\begin{aligned} V(X,Y,Z_0)=W_0(X',Y',Z')&\\ +2\sum_{g>0}[W_g^R(X',Y',Z')\cos 2\pi gN&\\ \times(Z'+h)/B+W_g^I(X',Y',Z')&\\ \times\sin 2\pi gN(Z'+h)/B]. \end{aligned} \tag{33}$$

This latter relation implies the following consequences.

(i) For $h=\pm b=\pm B/N$, one has

$$V(X,Y,Z_0)=V(X',Y',Z'). \tag{33'}$$

This relation defines the translational invariance of V due to the helix periodicity.

(ii) For $h=Z_0$, i.e., $Z'=0$, the interaction V between the helix and the probe atom located in a plane Z_0 can be determined in terms of the Fourier coefficients calculated in the plane $Z'=0$. This can be trivially shown by substituting $Z'=0$ in Eq. (33). Note furthermore that

$$V_0(X,Y,Z_0)=V_0(X',Y',0) \quad \text{for} \quad g=0, \tag{33''}$$

$$V(X,Y,Z_0)=V(X',Y',0) \quad \text{when } Z=nb,\ n \text{ integer}.$$

Moreover, from Eqs. (29) and (30), it may be seen that the interaction potential is invariant in the change $Y\rightarrow -Y$, when $Z_0=0$.

2. Calculations and results

The potential-energy surfaces between the probe atom and the helix are drawn for various characteristics of the helix and using the values of the Lennard-Jones coefficients given in Table II. Note that all the selected cases *a*–*d* correspond to b^* values smaller than 0.5 (cf. Table I) and that the potential coefficients are such that the probe atom can move inside the helix. In each case, the interaction energy V is determined for each set (X,Y) of the plane $Z=Z_0$. The potential-energy surface $V(X,Y,Z_0)$ is determined for a sampling of 1600 points (X,Y) with an interval $\Delta X=\Delta Y=0.5$ Å using either the standard sum procedure giving V_{AA} or the FTA leading to V. The truncation procedure on g for V is that used in Sec. IV A, the convergence criterium being $\delta\leqslant10^{-5}$ for the difference between V_{AA} and V. However, for some cases, δ cannot decrease even for large g values because of the rapid decrease of the Fourier coefficients with g; therefore, a second convergence criterium is

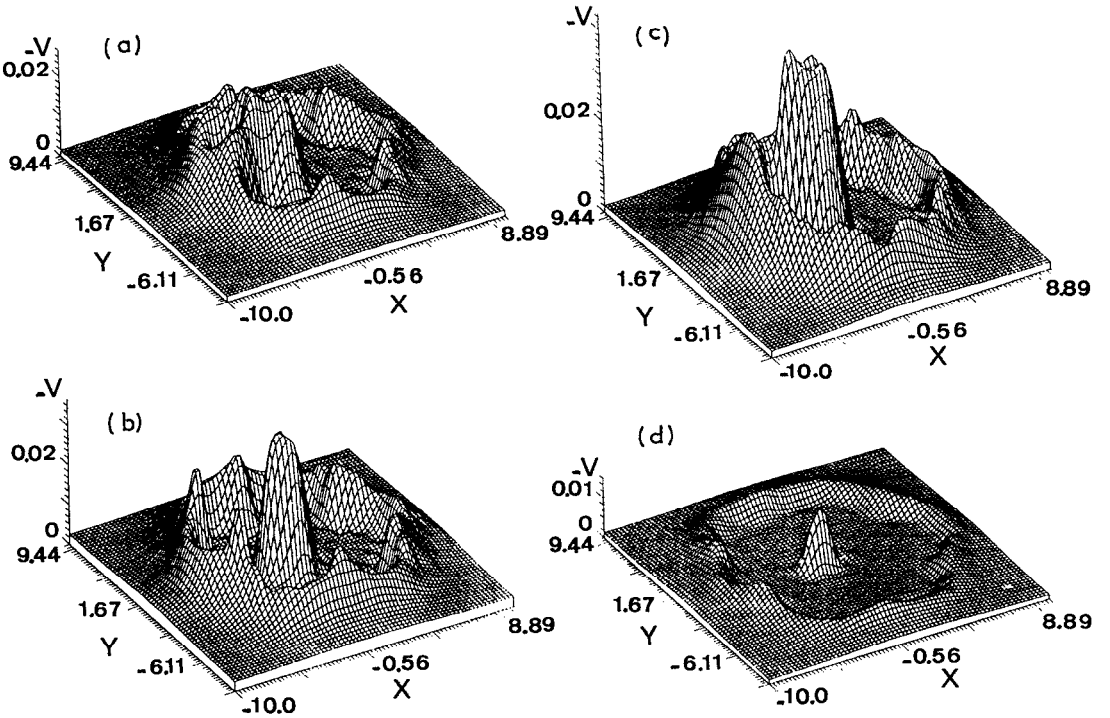

FIG. 3. Potential-energy surfaces $V_{AA}(X,Y)$ experienced by the probe atom moving in the plane $Z=0$ perpendicular to the helix axis. For clarity, we have drawn $-V=-V_{AA}$ and dropped to zero the repulsive values of V_{AA}. The surfaces (a)–(d) correspond to the parameter values given in Table II. Energy in eV, X and Y in Å.

used $|W_{g+1}|\leqslant 10^{-5}$. Note, moreover, that the potential-energy surfaces V_{AA} or V are identical for all planes $Z'=Z_0+nb$, being rotated by an angle $\theta_n=n2\pi/N$; it is thus only necessary to determine V in the range (Z_0,Z_0+b). For simplicity we take $Z_0=0$. The accuracy of the FTA is characterized by the absolute error $\Delta=\delta/|V_{AA}|$ for each surface set (X,Y).

Figures 3(a)–3(d) exhibit the potential-energy surfaces V_{AA} (X,Y) when the probe atom moves in the $Z=0$ plane. In fact, we represent $-V_{AA}$ and drop to zero the negative values of $-V_{AA}$ which would correspond to repulsive regions for the probe atom. Figures 3(a)–3(d) exhibit an attractive ring of potential corresponding to an outside position of the probe atom, then a repulsive part inside the ring which characterizes the helix matter, and a relatively sharp peak of attractive potential. This enhanced attractive potential region describes the fact that the probe atom lies inside the helix in its most stable configuration. Note that the potential-energy surface is not circularly symmetric due to the helicoidal structure. The attractive ring has also secondary peaks which correspond to the atom distribution along the helix. Their presence depends on the matter density and on the extent of the repulsive zone which prevents a close analysis of the helix by the probe atom. From Figs. 3(a)–3(c), the only changes are successively the decrease of the helix pitch and the increase of the atom number density along the helix which both lead to an increase of the matter density. The consequences of these changes are the increase of the secondary peaks in Figs. 3(b) with a concomitant increase of the interaction energy, whereas in Fig. 3(c) these minima nearly vanish and the potential surface looks like that of a continuum helix. In Fig. 3(d), the helix geometry is similar to the previous cases but the Lennard-Jones potential appears much more repulsive (Table II). The probe atom in that case cannot move close to the helix and it thus experiences the atom distribution as a helical continuum. This probe atom can, however, penetrate the helix to experience a stable position on the helix axis, but the interaction energy remains small when compared to the previous cases.

We have also considered the case a' where the A atoms moves inside a plane $Z=b/2$, i.e., without helix matter, using the same parameters as in case a. The same shape of the potential-energy surface is obtained but with an enhanced structure for the attractive ring with respect to the inside central peak.

The adequacy of the FTA for the calculation of the interaction potential V when compared to the standard sum procedure is exhibited in Table III for the absolute potential minimum. The g_m truncation is given for each case described in Table II, and it can be shown that the convergence is quite good for low g_m values, since accuracy is better than 3% for the less-favorable case, and the position of the minima is strictly the same for V_{AA} and V. Note, however, that for a small fraction (5%) of points in the repulsive zone which is, however, irrelevant for the adsorption process of the probe atom, the accuracy Δ can reach 15%.

A test of convergence is shown in Fig. 4, where we have drawn the zero Fourier coefficient only, leading to

TABLE III. Absolute minima for the probe-atom–helix interaction potential. Comparison of V_{AA} and V.

	X (Å)	Y (Å)	V_{AA} ($\times 10^{-1}$ eV)	V ($\times 10^{-1}$ eV)	g_m	Δ (%)
a	−2.5	±0.5[a]	0.242 612 9	0.235 694 3	2	2.85
	−2	±0.5[b]				
b	−1	±0.5	0.342 324 4	0.342 321 7	1	0
c	−2	0	0.471 388 6	0.471 388 6	1	0
d	−0.5	0	0.157 121 6	0.157 136 1	0	0.01
a'	−2	±1	0.232 475 2	0.237 054 4	3	1.97

[a]Calculated for the V_{AA} potential.
[b]Calculated for the V potential.

TABLE IV. Ratio of the zero Fourier coefficient and of the total energy in the Fourier analysis.

	$W_0/V\times 100$	$\overline{W_0/V}\times 100$	g_m
a	99.93	100.58	5
b	99.93	100.45	5
c	99.93	100.73	3
d	100.00	101.08	4
a'	100.00	100.84	3

$-V_0$, in case a of Tables II and III. This figure is to be compared with the results of Fig. 3(a). When the probe atom is far enough from the helix matter, the continuum approximation looks very good since the term $-V_0$ represents about 100% of the interaction V_{AA}. When the probe atom goes closer, the secondary minima are not well reproduced by $-V_0$ but, for the most stable positions, the agreement becomes, once again, satisfactory. The ratio W_0/V is given for each case a–a' in Table IV; these values correspond to the absolute minima of the potential-energy surface (column 2) or to average over all the explored points (column 3). The truncation values g_m of g are represented in Fig. 5 for case a in Table II. The boundaries of the various regions corresponding to a given g_m which satisfies the convergence criterium $\delta \leqslant 10^{-5}$ are schematized by solid lines. Most of the potential surface is well represented by the first two Fourier coefficients W_0 and W_1 and the whole potential surface is obtained for $g_m \leqslant 5$ (see Table IV). Note that the absolute minimum is reproduced with $g_m=2$ although the zone corresponding to the minimum is already obtained with $g_m=0$.

It is important to note that there is no evident correlation between the accuracy of the FTA and the g_m truncation. Indeed, large values of g_m are generally obtained at points of the potential-energy surface which correspond (i) to a sign change of the interaction, i.e., in the neighborhood of the repulsive region, and (ii) to secondary potential minima. To illustrate this feature, we compare the curves $V_{AA}(Y)$ and $V(Y)$ for $X=4$ Å, i.e., at the intersection of the plane $Z=0$ with the helix [Fig. 6(a)]. This case corresponds to the conditions of the first item (i) since $g_m=5$ is required for a Δ value equal to 83% when the probe atoms lies at $X=4$ Å and $Y=-5.5$ Å, i.e., close to the repulsive zone, while $g_m=3$ with $\Delta=7\%$ when the probe atom moves to $Y=-6$ Å. For $X=-5$ Å and Y varying from -10 Å to 0 [Fig. 6(b)] the probe atom experiences a region with a secondary potential minimum. The largest discrepancy between V_{AA} and V is calculated when $Y=-2$ Å since Δ reaches 36% with $g_m=4$, but decreases to 2% when the probe atom moves to $Y=-3.5$ Å with still $g_m=4$. From these results, we show that a largest truncation value for g_m does not necessarily provide a better accuracy.

V. CONCLUSION

The goal of this paper was to determine the accuracy of a Fourier-transform analysis of the interaction potential between an atom and a helicoidal distribution of atoms. This method has the invaluable computational advantage to be fast compared to the usual pairwise sum procedure when the atom moves along the helix axis. The potential-energy surfaces experienced by a probe atom which can lie outside and inside the helix lead to the following conclusions. The interaction energy calculated with the FTA is generally well represented by the first orders of the Fourier-series expansion.[5(b)] In particular, as already mentioned for planar surfaces, the zero Fourier coefficient provides the dominant contribution to the potential; it corre-

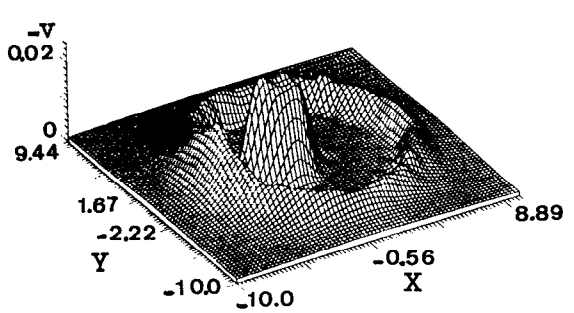

FIG. 4. Potential-energy surface $V_0=V(X,Y)$ experienced by the probe atom moving in a plane perpendicular to the helix axis (see Fig. 3), assuming that the helix is described by a continuum.

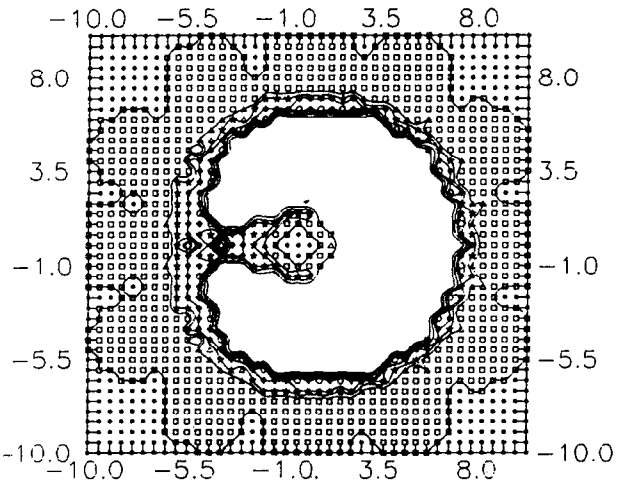

FIG. 5. Map of maximum values g_m of g required to get an accuracy δ better than 10^{-5} between V_{AA} and V; (●) $g_m=0$; (□) $g_m=1$; (△) $g_m=2$; (*) $g_m=3$; (✣) $g_m=4$; (○) $g_m=5$

sponds to the continuum description of the helix. Inside the helicoidal cavity, the accuracy of V is better than 2% with the contribution of the continuum term only for a reasonable matter density on the helix and appropriate geometrical helix parameters. Such an agreement is shown to be realized even for atom positions outside helix matter planes. It is thus expected that a continuum treatment of the helicoidal cavities containing a probe atom is quite convenient. Outside the helix, the accuracy depends on two main features: the atom–helix distance and the matter density of the helix. When the repulsive interactions prevent small atom–helix distances, the probe atom trivially feels a nearly continuum helix and particularly when the number density of atoms along the helix is large. Therefore, the Fourier-series expansion can be limited to very small g values. In the opposite case, and mainly in potential regions with local minima or sign changes, the convergence appears less good. Fortunately, such regions are generally irrelevant for the adsorption phenomena and an extension of the FTA to the whole potential region can be done.

A direct application of this numerical procedure to the atom or molecule adsorption in helicoidal micropore cavities of zeolites and related compounds and to the atomic probe of biological molecules could be performed.

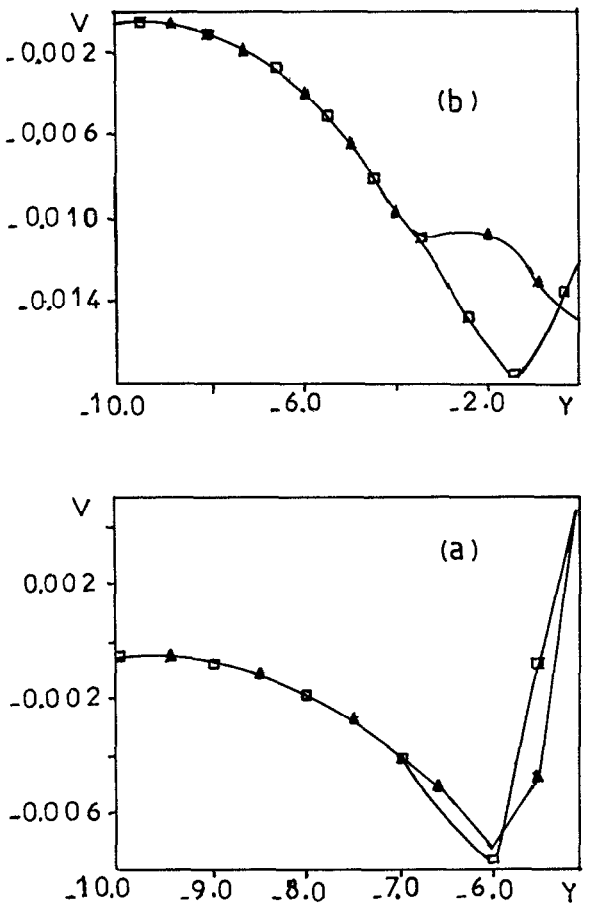

FIG. 6. Comparison of the behavior of V_{AA} and V vs Y for specific X positions of the probe atom: (a) $X=4$ Å; (b) $X=-5$ Å. The curves (□) and (△) correspond to V_{AA} and V, respectively.

[1] V. Bortolani, N. H. March, and M. Tosi, *Interaction of Atoms and Molecules with Solid Surfaces* (Plenum, New York, 1990).
[2] W. A. Steele, *The Interaction of Gases with Solid Surfaces* (Pergamon, Oxford, 1974).
[3] I. Derycke, J. P. Vigneron, Ph. Lambin, A. A. Lucas, and E. G. Derouane, J. Chem. Phys. **94**, 4620 (1991); T. Demi, *ibid.* **95**, 9242 (1991).
[4] J. Plata, J. Breton, and C. Girardet, Phys. Rev. B **38**, 3482 (1988); J. Plata, J. Breton, E. Alvira, V. Delgado, and C. Girardet, *ibid.* **43**, 5053 (1991).
[5] (a) Y. Okamoto, Y. Kaida, R. Aburatani, and K. Hatada, J. Chromatogr. **477**, 367 (1989); (b) E. Alvira, J. Breton, J. Plata, and C. Girardet, Chem. Phys. **118**, 233 (1987); **143**, 395 (1990); **155**, 7 (1991).
[6] P. Otto, E. Clementi, J. Ladik, and F. Martino, J. Chem. Phys. **80**, 5294 (1984); Y. Saruyama, *ibid.* **78**, 2077 (1983).
[7] I. S. Gradshteyn and I. M. Ryzhik, *Table of Integrals, Series and Products* (Academic, New York, 1980).